ACS APPLIED ENERGY MATERIALS

www.acsaem.org Article

Adhesive Polymers as Efficient Binders for High-Capacity Silicon Electrodes

Yiyang Pan, Sirui Ge, Zahid Rashid, Shilun Gao, Andrew Erwin, Vladimir Tsukruk, Konstantinos D. Vogiatzis, Alexei P. Sokolov, Huabin Yang,* and Peng-Fei Cao*

Cite This: *ACS Appl. Energy Mater.* 2020, 3, 3387−3396 Read Online

ACCESS | Metrics & More | Article Recommendations | Supporting Information

ABSTRACT: The major cause for capacity fading of silicon nanoparticle (SiNP)-based electrodes is the immense pressure applied toward the conductive networks during the charge/discharge process. While numerous efforts have been devoted to investigating different types of polymer binders, the rational design of an adhesive binder with pressure sensitivity has rarely been reported. Herein, a series of pressure-sensitive adhesives (PSAs) synthesized via copolymerization of 2-ethylhexyl acrylate (2-EHA) and acrylic acid (AA) are evaluated as polymer binders for SiNP-based electrodes. The balance between the density of interaction groups and viscoelastic properties is systematically investigated for efficient binding performance. The SiNP-based electrode using PSA with 20 mol % of 2-EHA (Si-PSA-20%) exhibits excellent electrochemical performance, achieving a capacity retention of 83% at the 100th cycle compared with 54% for Si-PAA after activation. Si-PSA-20% also delivers a superior cycling performance at a high current density (1731 mAh g^{-1} after 350 cycles vs 719 mAh g^{-1} after 150 cycles for Si-PAA, 1.8 A g^{-1}) and at high mass loading of active materials (capacity retention of 74 vs 38% for Si-PAA after 100 cycles, SiNP content ∼1.2 mg cm^{-2}). Atomic force microscopy (AFM), peel tests, and Car−Parrinello molecular dynamics (CPMD) simulations are employed to understand their binder performance. The novel design and systematical investigation of PSAs as binders will definitely be appealing for not only the Si electrode but also for other high-energy-density electrode materials.

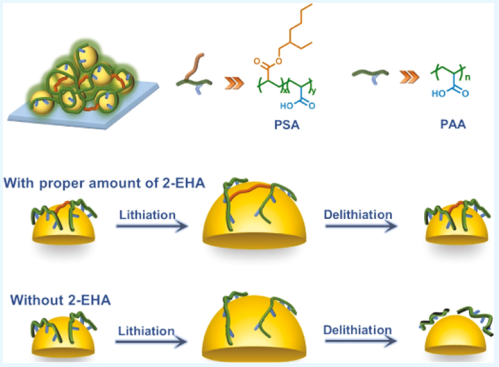

KEYWORDS: *polymer binder, pressure-sensitive, adhesive polymers, lithium-ion battery, silicon electrode*

1. INTRODUCTION

The rapid growth of electronic markets that depends on portable devices, electric vehicles, and energy storage grids has greatly promoted the development of advanced lithium-ion batteries (LIBs) with high energy density.[1,2] The conventional anode material, i.e., graphite, cannot fully meet this grand challenge due to its limited specific capacity (372 mAh g^{-1}).[3−6] On the other hand, the advent of alloy materials, including silicon (Si),[7−11] germanium (Ge),[12] and tin (Sn)[13] is promising for next-generation LIBs, owing to their excellent theoretical capacities (3579, 1384, and 994 mAh g^{-1}, respectively). Combined with its low electrochemical voltage and natural abundance, Si is extremely attractive as a high-energy-density anode material.[14,15] However, the large volume change (up to 300%) during the lithiation/delithiation process leads to the pulverization of Si particles, electrical isolation of active materials, and unstable solid electrolyte interface (SEI) layers. All of these in turn cause a rapid capacity fading of Si-based anodes.[16−19] Fabrication of Si with different nano-architectures, such as nanowires,[20] nanotubes,[21] thin films,[22,23] and porous structures[24] can efficiently improve the electrochemical performance of Si-based electrodes. However, assembling Si nanoparticles (SiNPs) into these specific structures usually requires complicated processes, high costs, and low scalability, thereby hindering their practical applications.[25]

The rational design of polymer binders is another efficient approach for improving the long-term electrochemical performance of SiNP-based electrodes, which is relatively cost-efficient.[26,27] The traditional polymer binder poly(vinylidene difluoride) (PVDF) shows poor performance as a binder material for SiNP-based electrodes due to its weak van der Waals force with the SiNP surface. Designing polymer binders to enable a stable conductive network around the active materials has been the key task for material scientists, while other parameters, such as electrochemical stability, mechanical robustness, less swelling in the electrolyte, and formation of a uniform slurry, are also vital in attaining excellent performance as binder components. The binders with

Received: December 11, 2019
Accepted: March 26, 2020
Published: March 26, 2020

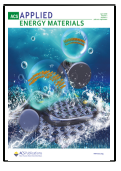

https://dx.doi.org/10.1021/acsaem.9b02420
ACS Appl. Energy Mater. 2020, 3, 3387−3396

a higher adhesion force to the SiNP surface, including covalent bonds and supramolecular interactions (such as hydrogen bonding and ionic bonding), can achieve SiNP-based electrodes with improved electrochemical performance and, therefore, many efforts have been devoted in this direction. For example, the polymers containing polar groups (e.g., −COOH and $-NH_2$), such as polyacrylic acid (PAA),[28,29] carboxymethyl cellulose (CMC),[30] alginate (Alg),[31] polyimide,[32] polyacrylonitrile,[33] poly(vinyl alcohol) (PVA),[34] carboxymethyl chitosan,[35] and guar gum (GG),[36] can form hydrogen bonding (or partial covalent bonding in some cases) with the hydroxyl groups on the surface of SiNPs. Sottos and co-workers developed a high-performance SiNP-based electrode, which exploited the dynamic ionic bonding between the carboxylic acid groups of PAA and amino-functionalized SiNPs.[37] A gel binder adhering to SiNPs by both covalent bonds and hydrogen bonds was reported by Song et al., and the gel showed better electrochemical performance than CMC, which only forms hydrogen bonding with SiNPs.[38] We also reported catechol-functionalized chitosan exhibiting coordination interaction with the SiNP surface, showing that only the binders with optimized grafting density of adhesion groups and crosslinking density allows efficient interaction with active materials.[39] Despite all of these efforts devoted in fabricating binder materials with an enhanced adhesion force with SiNPs, to the best of our knowledge, designing a pressure-sensitive adhesive (PSA) binder has rarely been reported. This type of study is especially attractive because the immense pressure of SiNPs applied toward the conductive network during the volume variation process is the major cause for the fading of capacity. The pressure sensitivity may allow the polymers to bond with SiNPs in a short time and resist debonding from the SiNP surface during the lithiation/delithiation process.[40]

PSAs have been widely used in many fields, including, but not limited to, packaging, electronic devices, and labels.[41] PSAs can bind to a substrate effectively with a little pressure and a short contact time, as well as resist debonding from the substrate (for example, keeping adhesion under large stress (>100%)).[42] Acrylic PSAs, which contain alkyl acrylate bases, are specifically attractive due to their inherent adhesion (i.e., they do not require additional compounding). 2-Ethylhexyl acrylate (2-EHA) is a common base for acrylic PSAs, and the properties of acrylic PSAs can be well-tuned by copolymerization with different monomers.[40,43] Considering the well-reported efficient interaction of carboxylic acid units with the SiNP surface, the acrylic PSA obtained by copolymerization of AA and 2-EHA should provide an efficient binder material that allows even a stronger adhesion force with SiNPs when applying pressure to the surrounding conductive networks (polymer binder and conductive additives) and maintain mechanical robustness during the following volume variation process. Another important parameter that has received little attention is the interaction of polymer binders with conductive additives (carbon black (CB) in most cases), which is also crucial to the ultimate cycling performance of nonconductive polymer binders.[44] The hydrophobic 2-EHA in the obtained polymer binders should also adhere to CB efficiently through hydrophobic interactions. To test the hypothesis, a series of acrylic PSAs with varied 2-EHA molar ratios were synthesized and investigated as binders for Si-based electrodes. As expected, the acrylic PSA with the optimized 2-EHA ratio exhibits significantly improved performance as a binder material for SiNP-based electrodes, with a capacity retention of 2372 mAh g^{-1} after 100 cycles at 360 mA g^{-1} and 1731 mAh g^{-1} after 350 cycles at a high current density of 1.8 A g^{-1} compared to those of 1710 mAh g^{-1} after 100 cycles at 360 mA g^{-1} and 719 mAh g^{-1} after 150 cycles at 1.8 A g^{-1} for the PAA binder, respectively. Moreover, the electrode with an optimized PSA binder content also delivers much better cycling stability at a high mass loading of SiNPs (∼1.2 mg cm^{-2}) compared with the PAA binder (capacity retention of 74 vs 38% after 100 cycles compared with the second cycle).

2. EXPERIMENTAL SECTION

2.1. Materials. 2-Ethylhexyl acrylate (2-EHA), acrylic acid (AA), and silicon (Si) were purchased from Aladdin. The electrolyte (EC/DEC = 1:1 by v/v, 1 M $LiPF_6$) was bought from DoDoChem, China. *n*-Butyl alcohol and ethyl alcohol were purchased from Bohua Chemical Reagent Limited Company, Tianjin, China.

2.2. Synthesis of PSAs. The typical synthesis of the PSAs follows the previous reports by Karnal et al.[45] Typically, 4 g of monomers with different molar ratios of 2-EHA and AA were dissolved in 8 g of *n*-butyl alcohol, followed by the addition of 40 mg of AIBN. The solution was degassed by purging with argon gas for 10 min before it was stirred at 65 °C for 24 h. After the reaction, the products were dialyzed against the mixture of water and ethyl alcohol (water/ethyl alcohol = 1:2 by volume) and followed by rotary evaporation. The obtained products were dried at 90 °C under vacuum for 12 h.

2.3. Preparation of Si Composite Electrodes. The Si−G composites were prepared by mixing 0.9 g of SiNPs and 2.1 g of graphite using ball-milling at a speed of 400 r/min for 12 h. The compositions of Si electrodes were 60 wt % active materials (SiNPs or Si−G composites), 20 wt % CB, and 20 wt % binder. PSA-10%, PSA-20%, PSA-50%, PSA-70%, PAA, and PVDF as different binders were investigated. Using PSA-20% as the polymer binder, the Si electrode with 70 wt % active materials, 15 wt % CB, and 15 wt % binder was also assembled for its cycling performance evaluation. Typically, 60 mg of the binder was dissolved in 2.5 mL of ethyl alcohol, and 180 mg of active material and 60 mg CB were added to the above solution. The mixture was magnetically stirred for 24 h. The slurry was coated on Cu foil with a doctor blade and dried under vacuum at 95 °C for 12 h. The mass loadings of SiNPs were ∼0.5 mg cm^{-2} for regular electrochemical tests and ∼1.2 mg cm^{-2} for high mass loading tests.

2.4. Characterization. ^1H NMR spectra were recorded on a Bruker 400 MHz NMR spectrometer using DMSO-*d*. Fourier-transform infrared spectroscopy (FT-IR) spectra were recorded on a Nicolet iS50 FT-IR Spectrometer (Thermo Scientific), and the scanning range was 4000−525 cm^{-1}. The atomic force microscopy (AFM) indentation was conducted according to the usual procedure on the OmegaScope, AIST-NT (Novato) scanning probe microscope using a colloidal silica probe (15 μm diameter) with a cantilever spring constant of 0.32 N m^{-1}.[39,46] For 180° peel tests, the electrode films (Si/binder/CB = 6:2:2 by weight) were prepared in the size of 12 × 30 mm^2 on Cu foils, and 3M-tape was attached onto them. The 180° peel tests were performed using a universal test machine (MTS) at a speed of 100 mm min^{-1}. The X-ray diffraction (XRD) was performed on Rigaku D/max-2500 X. The transmission electron microscopy (TEM) images of Si and electrodes were characterized by high-resolution transmission electron microscopy (JEM-2800), and scanning electron microscopy (SEM) images and SEM−energy dispersive X-ray spectroscopy (EDS) mapping images were obtained from the field emission scanning electron microscope (JSM-7800F). Electrochemical impedance spectroscopy (EIS) was measured from 10 mHz to 100 kHz with a Zennium Pro. The cyclic voltammetry was conducted with the Zennium Pro at a constant rate of 0.1 mV s^{-1}. Thermogravimetric analysis (TGA) was carried out on a Q-50 thermogravimetric analyzer (TA Instrument), and different scanning calorimetry (DSC) was performed on a Q-2500 differential scanning calorimeter (TA Instrument). Small-amplitude oscillatory shear measurements were performed with a strain-controlled mode of the AR2000ex (TA Instruments) in an angular frequency range of 10^{-1}−

https://dx.doi.org/10.1021/acsaem.9b02420
ACS Appl. Energy Mater. 2020, 3, 3387−3396

10^{-2} rad/s using parallel plate geometry, with a disk diameter of 4 mm. The reference temperature is 90 °C, and the temperature ranges of PSA-10%, PSA-20%, PSA-50%, and PSA-70% were 95−150, 80−150, 20−120, and −35−70 °C, respectively.

2.5. Electrochemistry. The cycling process was performed using CR2032-type coin cells with lithium foil as the counter electrode and Celgard 2400 as the separator. The cells were assembled in an argon-filled glovebox (<0.1 ppm of both water and oxygen). The electrolyte was a mixture of EC and DEC (1:1 by volume) with 1 mol/L $LiPF_6$ salt, and 10 wt % fluoroethylene carbonate (FEC) was added to the electrolyte as the electrolyte additive. Galvanostatic charge−discharge cycling tests were conducted with a LAND automatic battery cycler. The charge−discharge process was performed between 3 and 0.01 V vs Li/Li^+.

2.6. Computational Simulations. To check the binding of AA and 2-EHA copolymer on the silica surface, Car−Parrinello molecular dynamics simulations were performed within the plane-wave formalism as implemented in QUANTUM ESPRESSO.[47] We used norm-conserving Martins−Troullier pseudopotentials with the Becke−Lee−Yang−Parr (BLYP) exchange−correlation functional.[48,49] The plane-wave energy cutoff was set to 30 Ry. All simulations were performed in the NVT ensemble using the Nose−Hoover thermostat at 300 K and a 20 fs time step for 200 ps. The system was modeled using AA and 2-EHA copolymer on the surface of a silica slab. In the molecular dynamics (MD) simulations, the atoms of the slab were kept fixed and only the atoms of the polymers were allowed to move.

3. RESULTS AND DISCUSSION

3.1. Fabrication of PSA Containing SiNP-Based Electrodes. Scheme 1 shows the copolymerization of AA and 2-EHA, and a series of polymers with different 2-EHA ratios (10, 20, 50, and 70 mol %, denoted as PSA-10%, PSA-20%, PSA-50%, and PSA-70%, respectively) were synthesized at 65 °C in *n*-butyl alcohol (see details in the Experimental Section). With difficulty in obtaining the reliable data for number-average molecular weight (M_n) and polydispersity (PDI) of all samples due to the presence of a large number of carboxylic acid groups, the gel permeation chromatography (GPC) data of PSA-70% (M_n = 22.2 kDa, PDI = 2.74), as a typical example, is as shown in Table S1. As illustrated by the FT-IR spectra in Figure S1, the peaks at 1692 and 1455 cm^{-1} are attributed to the C═O stretching and C═O bending, respectively, in −COOH groups, verifying the presence of AA segments. It should be noted that the intensity of the peak at 2931 cm^{-1}, which is ascribed to the C−H stretching in the $-CH_2$ or $-CH_3$ groups on the 2-EHA, gets higher following the increased molar ratios of 2-EHA contents, consistent with previous reports.[50] Moreover, as shown in the ^1H NMR spectra of PSAs, PAA, and poly(2-EHA) (Figures 1A and S2−S6), the integration of peak b, which corresponds to the proton of carboxylic acid, decreases with the increased molar ratios of 2-EHA when fixing the peak integration of $-CH_2$ units adjacent to the ester group, confirming the successful synthesis of the copolymers with different 2-EHA ratios.

Scheme 1. (A) Synthesis of PSAs with Varied 2-EHA Ratios. (B) Illustrating the Impact of PSA Binders on the SiNP Surface

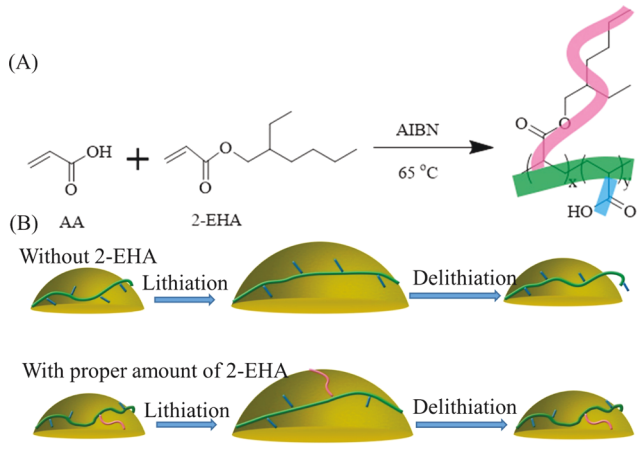

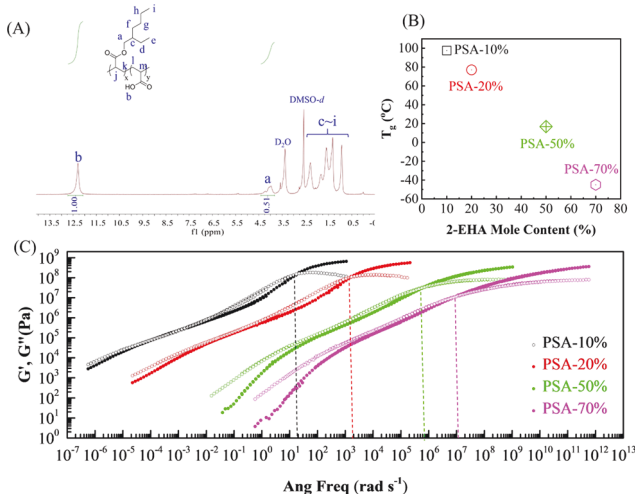

Figure 1. (A) ^1H NMR spectrum of PSA-10%. (B) Glass transition temperature (T_g) of polymers with different molar contents of 2-EHA. (C) Frequency dependence of the storage moduli (G') (close symbols) and loss of storage moduli (G'') (open symbols) of PSA-10%, PSA-20%, PSA-50%, and PSA-70% using the time-temperature superposition at the reference temperature of 90 °C.

No thermal decomposition was observed for all PSAs until 300 °C, as measured by thermogravimetric analysis (TGA, Figure S7), indicating the high thermal stability of the polymers in the temperature range of the operating batteries. As illustrated by different scanning calorimetry (DSC), the glass transition temperature (T_g) of PSA-10%, PSA-20%, PSA-50%, and PSA-70% decreased from 97.5 to −45.0 °C (as plotted in Figure 1B, details in Figure S8), suggesting the tunable T_g values of PSAs by varying the 2-EHA contents. A polymer with a lower T_g value usually means a more ductile nature at a given temperature[51] and, therefore, the incorporation of 2-EHA endows the carboxylic acid-based polymer binders with improved flexibility. The frequency dependence of the oscillatory shear moduli for storage moduli (G') and loss moduli (G'') of the PSAs using time−temperature superposition at the reference temperature of 90 °C are shown in Figure 1C. The polymer behavior is controlled by the viscoelastic nature, which can be divided into the elastic component, depicted by G', and the viscous component, described by G''.[52] Segmental relaxation time τ was estimated using the following equation

$$\tau = \frac{1}{\omega_c}$$

where ω_c is determined from the crossover angular frequency, where G' and G'' intersect (marked by dashed lines in Figure 1C).[53] The PSAs with higher 2-EHA molar ratios show a

https://dx.doi.org/10.1021/acsaem.9b02420
ACS Appl. Energy Mater. 2020, 3, 3387−3396

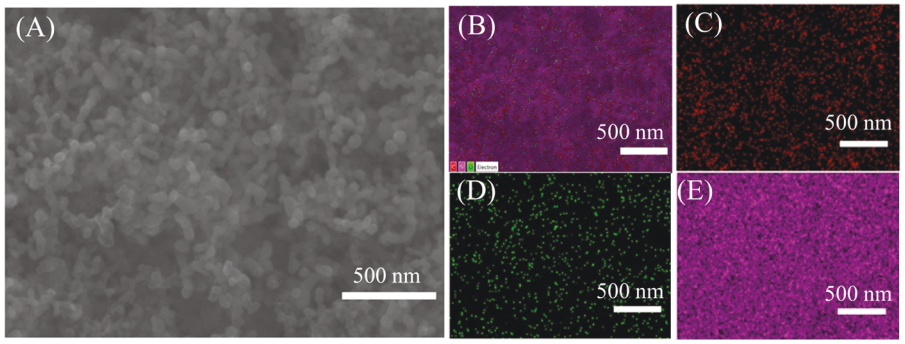

Figure 2. (A) SEM mapping image of the SiNP-based electrode with the PSA-20% binder before cycling. (B)−(E) are the corresponding SEM−energy-dispersive X-ray spectroscopy (SEM−EDS) mapping images ((C)−(E) correspond to C, Si, and O elements, respectively).

shorter segmental relaxation time, indicating faster segmental motion at the same temperature. This is consistent with the decreased T_g values following the increased molar ratios of 2-EHA for PSAs. The tensile tests also demonstrate the flexible nature of PSAs due to the presence of 2-EHA contents, and as shown in Figure S9, the obtained polymers with higher 2-EHA ratios exhibit higher elongation before breaks.

The SiNP-based electrodes were prepared with 60 wt % active materials (SiNPs or SiNP-graphite composites), 20 wt % polymer binder, and 20 wt % CB. The scanning electron microscopy (SEM) and transmission electron microscopy (TEM) images (Figure S10) reveal the SiNPs with an average diameter of 70 nm. The X-ray diffraction (XRD) patterns (Figure S11) verify the cubic crystalline nature of the commercial SiNPs.[54] The SEM−energy-dispersive X-ray spectroscopy (SEM−EDS) mapping demonstrates the presence of the SiO_2 layer on the SiNP surface, whose terminal hydroxyl groups are crucial for the formation of strong adhesion between active materials and polymer binders,[55] in accordance with the previous reports.[56] To investigate the distribution and homogeneity of the active materials and the PSA binder (i.e., PSA-20%), the SEM−EDS elemental mappings were also carried out. As manifested by Figure 2A−E, the Si, C, and O elements are homogeneously distributed in the electrode, demonstrating the even distribution of active materials, carbon additives, and polymer binders (see the ratio of the element content in Figure S12).

3.2. Performance of PSAs with Different 2-EHA Contents as Binder Materials. The electrochemical performance of SiNP-based electrodes was evaluated by the galvanostatic test with lithium metal as the counter electrode. Fluoroethylene carbonate (FEC) (10 wt %) was also added in the electrolyte solution (1 M $LiPF_6$ in ethylene carbonate/dimethyl carbonate (EC/DEC), 1:1 by volume) to facilitate the formation of a stable SEI layer.[57] The charge/discharge process of the SiNP-based electrodes was performed between 0.01 and 3 V using CR2032 coins. PSA-70% was initially tested for its performance as a binder material in SiNP-based electrodes because our initial assumption is its excellent viscoelastic performance, e.g., over 2000% elongation before breaks (see Figure S13), may contribute to the enhanced electrochemical performance during the volume variation process of active materials.[54] As shown in Figure 3C, though improved cycling performance is achieved compared with the electrode with PVDF (the capacity retention of 38 vs 6.8% at the 100th cycle at a current density of 360 mA g^{-1}, compared with the cycle after the activation (initial cycle)), the SiNP-based electrode using PSA-70% as the binder (named Si-PSA-70%) still exhibits unsatisfactory cycling behavior. The possible explanation is that the interactions between PSA-70% and the SiNP surface are still dominated by weak van der Waals forces, because the polymers with a high density of aliphatic chains may hinder the efficient interaction between carboxylic acid groups and the Si surface.

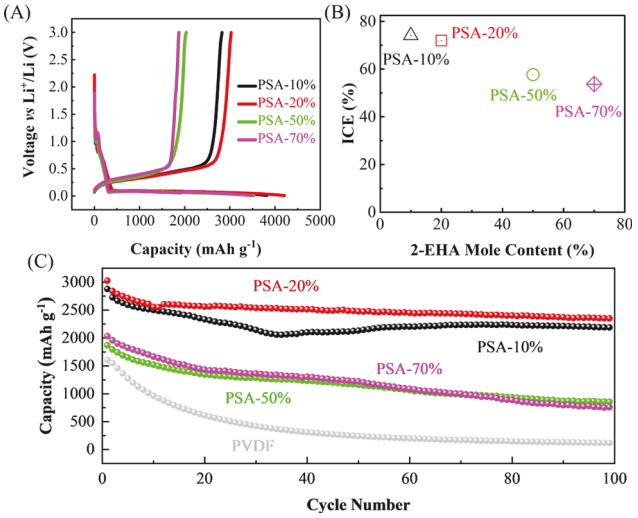

Figure 3. (A) Voltage profiles of different electrodes at the initial cycle. (B) Initial Coulombic efficiencies (ICE) of Si-PSA-10%, Si-PSA-20%, Si-PSA-50%, and Si-PSA-70%. (C) Comparative cycling performance of SiNP electrodes with PSA-10%, PSA-20%, PSA-50%, PSA-70%, and PVDF as binders at a current density of 360 mA g^{-1}.

Therefore, the PSAs with lower 2-EHA contents were further evaluated for their electrochemical performance, considering the reduced steric effect on forming efficient interaction with the SiNP surface. Figure 3C shows the comparative cycling performance of SiNP-based electrodes using PSAs with different 2-EHA contents as binders at a current density of 360 mA g^{-1}. Si-PSA-10%, Si-PSA-20%, Si-PSA-50%, and Si-PSA-70% exhibit the initial delithiation capacities of 2827, 3028, 1870, and 2034 mAh g^{-1}, and capacity retentions of 80, 83, 48, and 38% at the 100th cycle, respectively. Among this series of electrodes with different PSA binders, Si-PSA-20% delivers the best cycling performance with a retention capacity reaching 83% after 100 cycles. The voltage profiles of SiNP-based electrodes with different binders during the initial lithiation/delithiation process are shown in Figure 3A. Lithiation is represented by the plateaus at 0.15 V during the discharge process, and delithiation is described by the plateaus at 0.4 V during the charge process.[58] As shown in

https://dx.doi.org/10.1021/acsaem.9b02420
ACS Appl. Energy Mater. 2020, 3, 3387−3396

Figure S14, Si-PSA-20% has typical lithiation and delithiation peaks, which are consistent with the previous studies.[36] The initial Coulombic efficiencies (ICE) of these SiNP electrodes with PSA-10%, PSA-20%, PSA-50%, and PSA-70% were calculated to be 74, 72, 58, and 54%, respectively, as shown in Figure 3B, indicating that the high content of 2-EHA may hinder the efficient formation of a stable SEI layer during the initial cycle.

The comparative performance of PSAs with different 2-EHA contents as binder materials can be explained by the two key parameters, i.e., the density of adhesion groups and viscoelastic properties. With the increasing ratio of 2-EHA, the PSAs show more liquid-like behavior that was confirmed by the faster segmental relaxation (Figure 1C). The faster segmental relaxation of the binders with high 2-EHA contents should contribute to the good wettability on the active materials, which is of crucial importance for improved electrochemical performance.[53] However, considering the van der Waals force between 2-EHA and the SiO_2 surface, the PSAs with higher molar ratios of 2-EHA may eliminate the efficient interaction of polymers with the SiNP surface, which may prevent the formation of a stable conductive network.[37] Therefore, there should be a balance between the density of adhesion groups and viscoelastic properties for efficient electrochemical performance. In view of the surface on the SiNPs covered with the SiO_2 layer, atomic force microscopy (AFM) measurements were conducted on the PSAs using the SiO_2 probe to provide insight into the adhesion force of PSAs with the Si surface, as shown in Figure 4A. With more liquid-like

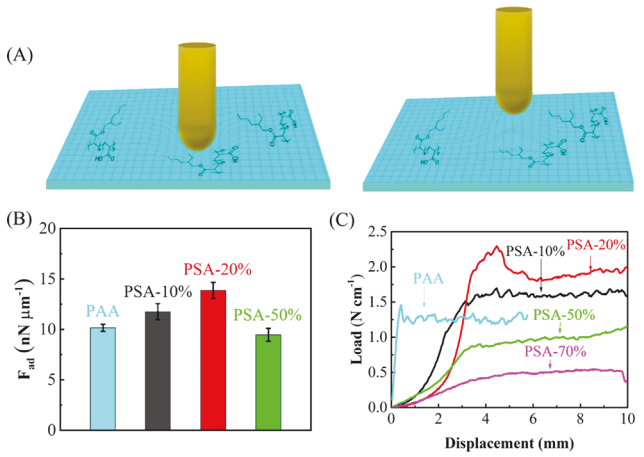

Figure 4. (A) Illustration of the adhesion test between the SiNP surface and polymer binders by atomic force microscopy (AFM). (B) Comparative adhesion forces (F_{ad}, normalized by the probe size) of PAA, PSA-10%, PSA-20%, and PSA-50% with the SiO_2 surface measured by AFM. (C) Comparable peel strength of electrodes with PAA, PSA-10%, PSA-20%, PSA-50%, and PSA-70% as binders.

behavior as discovered by the rheology test (T_g = −45.0, 16.8, 77.0, and 97.5 °C for PSA-70%, PSA-50%, PSA-20%, and PSA-10%, respectively), PSA-70% is too soft/sticky to be measured by AFM. As shown in Figure 4B, PSA-20% delivers the highest adhesion force among the measured PSA samples. Though the test conditions cannot be the same as the environment inside the cells, the results can still provide useful information to explain the excellent electrochemical performance of the Si-PSA-20% electrode. This may be the result of the balance between the viscoelastic properties and the density of carboxylic acid groups. The pressure-sensitive adhesion allows more efficient interactions with SiNPs, which also enhances the adhesion strength with SiNPs, especially for the polymers possessing the suitable viscoelasticity.[59] The peel strength between the electrode composites and current collector is another important parameter for their ultimate electrochemical performance, which also relies on the density of adhesion groups and viscoelastic properties, as demonstrated in our previous report.[39] The 180° peel tests show that the electrode with PSA-20% delivers the highest peel strength with copper foil (see Figure 4C). In this case, the improved binder performance is mainly contributed to the enhanced adhesion force with both active materials and the current collector, which plays an important role in maintaining a stable conductive network during the cycling process.

3.3. Performance of PSA-20% as a Binder Material.

PAA is one of the state-of-art nonconductive polymer binders for SiNP-based electrodes, which shows much better electrochemical performance than PVDF and CMC.[28,60] To further substantiate the performance of PSA-20% as a binder material for SiNP-based electrodes, PAA was utilized as a control. As shown in Figure 5A, the electrode Si-PSA-20% exhibits

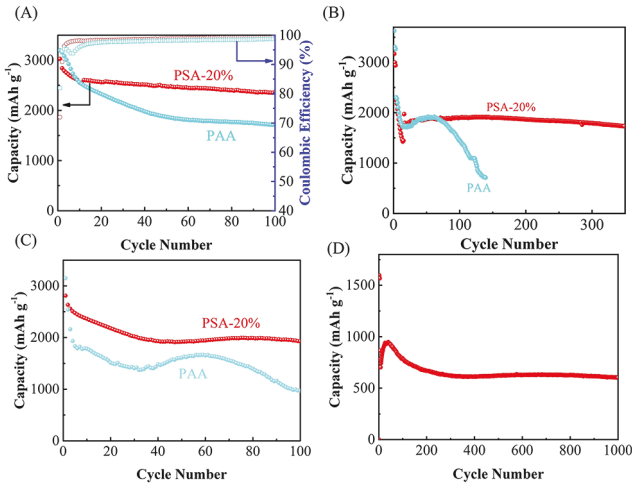

Figure 5. (A) Cycling performance of Si-PSA-20% and Si-PAA at a current density of 360 mA g^{-1}. (B) Cycling performance of Si-PSA-20% and Si-PAA at a high current density of 1.8 A g^{-1}. (C) Cycling performance of SiNP-based electrodes with a high mass loading of Si (~1.2 mg cm^{-2}) at a current density of 360 mA g^{-1}. (D) Long-term cycling performance of Si-G-PSA-20% at a current density of 1800 mA g^{-1}.

significantly improved electrochemical stability compared with that of Si-PAA (capacity retention of 83 vs 54%) at the 100th cycle at a current density of 360 mA g^{-1}. Even at a current density of 1.8 A g^{-1} (180 mA g^{-1} for initial three cycles), Si-PSA-20% still delivers a reversible capacity of 1731 mAh g^{-1} after 350 cycles. On the contrary, the capacity of Si-PAA drops rapidly to 719 mAh g^{-1} after 150 cycles at the same current density (see Figure 5B), and the trend is in agreement with the previous reports.[28] The capacity increases for the first few cycles at the current density of 1.8 A g^{-1}, which is most probably due to the electrode polarization. The Si-PSA-20% electrode with high mass loading of active materials (~1.2 mg cm^{-2}) was also fabricated to test its electrochemical performance. As shown in Figure 5C, the obtained electrode exhibits an initial delithiation capacity of 2811 mAh g^{-1} and a capacity

https://dx.doi.org/10.1021/acsaem.9b02420
ACS Appl. Energy Mater. 2020, 3, 3387−3396

retention of 74% at the 100th cycle in comparison with only 38% for the electrode with comparable mass loading of SiNPs but the PAA binder. The rate performance of Si-PSA-20% is shown in Figure S15, and the specific capacities can reach 1068 and 650 mAh g^{-1} at high current densities of 3.6 and 4.0 A g^{-1}, respectively. When lowering the current density to 360 mA g^{-1}, the specific capacity of 2946 mAh g^{-1} is obtained. Furthermore, the electrode Si-PSA-20% with 70 wt % of Si also possesses a stable cycling performance with a retention capacity of 2184 mAh g^{-1} after 100 cycles at a current density of 360 mA g^{-1} (Figure S16). The SiNP−graphite (Si−G) composites are more attractive for practical applications due to the high areal capacity, mature production process, and low cost compared to exclusive utilization of SiNPs as active materials.[51,61] Therefore, the electrode using Si−G composites (70 wt % graphite and 30 wt % Si) was also made to test its electrochemical behavior. As shown in Figure S17, Si-G-PSA-20% delivers a capacity retention of 1198 mAh g^{-1} at the 100th cycle, higher than that of Si-G-PAA (1054 mAh g^{-1} at the 100th cycle). Though cycling stability is not improved compared with Si-G-PAA, the higher capacity of Si-G-PSA-20% should be contributed by the higher adhesion force with graphite due to the hydrophobic interactions. Furthermore, at a high current density of 1.8 A g^{-1}, Si-G-PSA-20% still exhibits a reversible capacity of 606 mAh g^{-1} after 1000 cycles (Figure 5D), which may even meet the cycle number of practical applications.

The enhanced adhesion force of the pressure-sensitive adhesive, i.e., PSA-20%, with active materials and current collectors, may be the primary reason for its improved electrochemical performance. It is reported that the improved adhesion strength of polymers with SiNPs may promote the formation of a thinner SEI layer on SiNPs,[39] and higher adhesion force of PSA-20% with SiNPs compared with PAA may contribute to a thinner and more stable SEI layer. Though with less amount of carboxylic acid groups, the optimal viscoelastic properties may allow PSA-20% with a stronger adhesion force with the SiNP surface as provided by AFM measurements (Figure 4B). Considering the immense pressure applied to the surrounding conductive networks during the volume variation process of SiNPs, the pressure-sensitive adhesion may also contribute to forming a stronger adhesion force with SiNPs. Car−Parrinello molecular dynamics (CPMD) simulations were also employed to study the adhesion force between the silica surface and PSA or PAA, as shown in Figure 6. The polymers are periodic systems and only unit cells were considered to study their binding energies with the silica surface. The silica is selected because the SiNP surface is covered by SiO_2. The computation results show that the PSA (2-EHA/AA ratio being 1:5) has a much higher binding energy to silica than that of PAA (−12.4 vs −2.1 kcal mol^{-1}). The higher binding energy of PSA-20% is due to favorable hydrogen interactions with the oxygen atoms on the silica surface. The long chain of 2-EHA in PSA-20% has many hydrogen atoms, which can adjust on the surface and interact with oxygen atoms of the surface. These interactions are absent in the PAA, partially due to the lesser availability of the surface-oxygen atoms in the vicinity and high rigidity of the silica surface. Though the calculation cannot be performed in the real environment of a working cell, the result can still provide evidence for the higher adhesion force of PSA-20% with SiNPs. The coverage around SiNPs is illustrated by scanning transmission electron microscopy (STEM) (Figure 7B,C, corresponding TEM images in Figure S18), and the PSA-20% binder uniformly covers on the Si surface at the 10th cycle. Although the Si-PSA-20% system has a lower ICE than Si-PAA (72 vs 82%), the relatively higher average CEs of Si-PSA-20% (98.4 vs 97.6% for 100 cycles) also confirm the formation of a more stable SEI layer when using the PSA-20% binder.

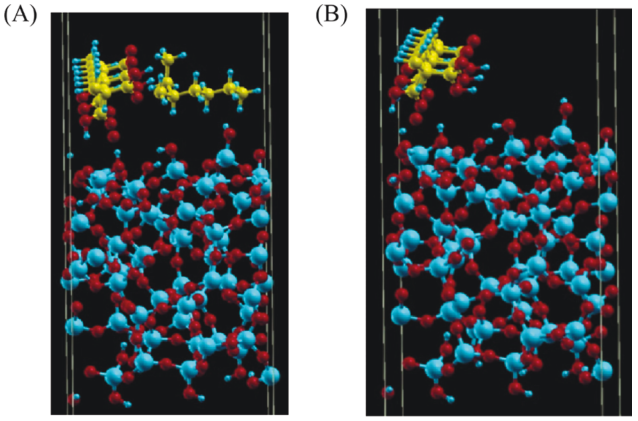

Figure 6. Optimized geometries from CPMD simulations for the polymers with (A) AA/2-EHA = 5:1 and (B) AA/2-EHA = 6:0.

The enhanced adhesion force with SiNPs may contribute significantly to maintaining the conductive networks and mechanical integrity of the electrodes during the volume variation process of the active materials (see Figure 7A). The morphologies of electrodes with different binders before and after 100 cycles were visualized by SEM mappings. As seen in Figure 7D−G, the electrode Si-PSA-20% exhibits slight cracking after 100 cycles, while severe cracks are observed in the electrode Si-PAA after the same cycling process. As illustrated by the electrochemical impedance spectroscopy (EIS) results in Figures S19 and S20, though the impedance values of Si-PSA-20% are higher than those of Si-PAA due to the lower Li-ion conductivity, the resistance of Si-PSA-20% is more stable during the cycling process, which manifests the stable SEI layer and conductive networks. The curves contain a semicircle in the high-frequency range, and a line in the low-frequency range follows the semicircle. Furthermore, the electrode Si-PSA-20% also shows improved peel strength to the current collector compared to PAA as confirmed by the 180° peel tests (see Figure 4C), and the results indicate that the electron transfer to the current collector may be more efficient during the cycling process.

The other properties of PSA-20%, like fast polymer dynamics and improved interactions with the conductive networks, also play important roles in its improved electrochemical performance. As shown in Figure 1C, the PSA-20% delivers a decent segmental relaxation time, while the rheology test of PAA cannot be performed at the same temperature range due to its high T_g value. The faster chain dynamics of PSA-20% should provide a relatively rapid response to external stress during the cycling process. The combination of the hydrophobic 2-EHA and hydrophilic AA, which constitute an amphiphilic structure also allows enhanced adhesion strength of PSA-20% with the carbon additives such as CB via hydrophobic interaction, which is also vital to preserve the stability of the conductive networks.[44] To explore the interaction between PSA-20% and CB as well as PAA and CB, solution A (contained 60 mg PSA-20%, 60 mg CB, and 2.5

https://dx.doi.org/10.1021/acsaem.9b02420
ACS Appl. Energy Mater. 2020, 3, 3387−3396

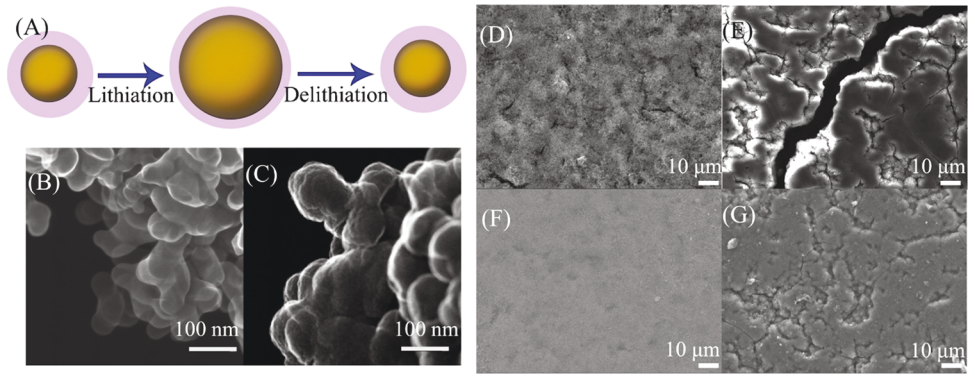

Figure 7. (A) Illustration on the impact of the PSA-20% binder in the SiNP-based electrode. The STEM images of electrodes with PSA-20% (B) before cycle and (C) at the 10th cycle. The SEM images of the Si-PAA electrode (D) before cycle and (E) at the 100th cycle. The SEM images of the Si-PSA-20% electrode (F) before cycling and (G) at the 100th cycle.

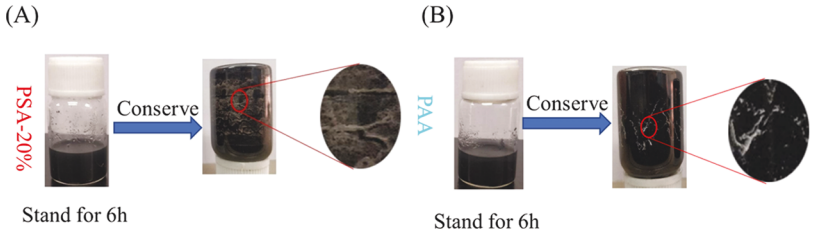

Figure 8. (A) and (B) demonstrate the comparative interaction of PSA-20% and PAA with carbon black. After standing for 6 h, the two bottles were conserved quickly. (A) Bottle A with the PSA-20% solution was homogeneous, most of the CB went down with the PSA-20% solution, and only a few CB was deposited on the wall of the bottle, indicating the higher interaction force of PSA-20% with CB. (B) Large amount of CB was deposited on the wall of the bottle B with PAA solution, indicating the low adhesion force of PAA with CB.

mL ethyl alcohol) and solution B (contained 60 mg PAA, 60 mg CB, and 2.5 mL ethyl alcohol) were stirred for 1 h to obtain a homogeneous dispersion. As shown in Figure 8A,B, after standing for 6 h, bottle A and bottle B were conserved. The CB in bottle A was dispersed well, while most of the CB in bottle B was inclined to stick on the inner surface of the vial. This simple demonstration shows that the adhesion force of PSA-20% to CB may be higher than that of PAA.

4. CONCLUSIONS

A series of pressure-sensitive adhesives have been synthesized and tested as binder materials for SiNP-based electrodes, and the PSA with an optimal 2-EHA content exhibits an improved adhesion force with both active materials and conductive additives, achieving an excellent performance as a binder component. Modifying the molar ratios of 2-EHA and AA allows control of the viscoelastic properties and the efficient interactions of PSAs with active materials, which are the two key parameters of their performance as binder materials. The SiNP electrode using the binder with an optimal content of 2-EHA, i.e., PSA-20%, delivers a high initial delithiation capacity (3028 mAh g^{-1}) and excellent retention capacity at different current densities (2372 mAh g^{-1} at the 100th cycle at 360 mA g^{-1} and 1731 mAh g^{-1} at the 350th cycle at 1800 mA g^{-1}). The PSA-20% also enables the high-performance Si electrode with high mass loading of active materials (1925 mAh g^{-1} after 100 cycles at 360 mA g^{-1} with mass loading of SiNP ~1.2 mg cm^{-2}) and the Si−G composite electrode (70 wt % graphite and 30 wt % Si, 606 mAh g^{-1} at 1.8 A g^{-1} after 1000 cycles). The adhesion force of PSAs or PAA with active materials has been verified by the AFM test and CPMD simulations. It is anticipated that the adhesive binder design using the pressure variation of active materials will be not only limited to a high-capacity silicon electrode but also to other high-energy-density electrode materials that suffer from severe volume change during the charging/discharging process.

■ ASSOCIATED CONTENT

Supporting Information

The Supporting Information is available free of charge at https://pubs.acs.org/doi/10.1021/acsaem.9b02420.

Additional material characterization and electrochemical performance; results of gel permeation chromatography (GPC) for PSA-70%; ^{1}H NMR spectrum of PAA; thermogravimetric analysis (TGA) curves of PSA-10%, PSA-20%, PSA-50% and PSA-70%; scaning electron microscopy (SEM) image of the commercial SiNPs; X-ray diffraction (XRD) patterns of commercial SiNPs; cyclic voltammetry (CV) measurements of Si composite electrode with PSA-20% binder (PDF)

■ AUTHOR INFORMATION

Corresponding Authors

Huabin Yang − *Institute of New Energy Material Chemistry, School of Materials Science and Engineering and Tianjin Key Laboratory of Metal and Molecule Based Material Chemistry, Nankai University, Tianjin 300350, China*; Email: hb_yang@nankai.edu.cn

Peng-Fei Cao − *Chemical Sciences Division, Oak Ridge National Laboratory, Oak Ridge, Tennessee 37830, United States*; orcid.org/0000-0003-2391-1838; Email: caop@ornl.gov

https://dx.doi.org/10.1021/acsaem.9b02420
ACS Appl. Energy Mater. 2020, 3, 3387−3396

Authors

Yiyang Pan − *Institute of New Energy Material Chemistry, School of Materials Science and Engineering, Nankai University, Tianjin 300350, China*

Sirui Ge − *Department of Materials Science and Engineering, University of Tennessee, Knoxville, Tennessee 37996, United States*

Zahid Rashid − *Department of Chemistry, University of Tennessee, Knoxville, Tennessee 37996, United States*

Shilun Gao − *Institute of New Energy Material Chemistry, School of Materials Science and Engineering, Nankai University, Tianjin 300350, China*

Andrew Erwin − *Chemical Sciences Division, Oak Ridge National Laboratory, Oak Ridge, Tennessee 37830, United States; School of Material Science and Engineering, Georgia Tech, Atlanta, Georgia 30332, United States*

Vladimir Tsukruk − *School of Material Science and Engineering, Georgia Tech, Atlanta, Georgia 30332, United States;* orcid.org/0000-0001-5489-0967

Konstantinos D. Vogiatzis − *Department of Chemistry, University of Tennessee, Knoxville, Tennessee 37996, United States;* orcid.org/0000-0002-7439-3850

Alexei P. Sokolov − *Department of Chemistry, University of Tennessee, Knoxville, Tennessee 37996, United States; Chemical Sciences Division, Oak Ridge National Laboratory, Oak Ridge, Tennessee 37830, United States;* orcid.org/0000-0002-8187-9445

Complete contact information is available at: https://pubs.acs.org/10.1021/acsaem.9b02420

Notes

The authors declare no competing financial interest.

■ ACKNOWLEDGMENTS

This work was financially supported by the Natural Science Foundation of China (21421001), the Natural Science Foundation of Tianjin, China (18JCZDJC31400), and the MOE Innovation Team (IRT13022). P.-F.C., S.G., A.E., and A.P.S. acknowledge partial financial support for FT-IR, rheological, and AFM measurements, data analysis and manuscript revision by the U.S. Department of Energy, Office of Science, Basic Energy Science, Material Science and Engineering Division. Z.R. and K.D.V. would like to acknowledge the University of Tennessee for financial support of this work (start-up funds) and the Advanced Computer Facility (ACF) of the University of Tennessee for computational resources.

■ REFERENCES

(1) Jin, Y.; Hu, C.; Dai, Q.; Xiao, Y.; Lin, Y.; Connell, J. W.; Chen, F.; Dai, L. High-Performance Li-CO_2 Batteries Based on Metal-Free Carbon Quantum Dot/Holey Graphene Composite Catalysts. *Adv. Funct. Mater.* **2018**, *28*, No. 1804630.

(2) Li, Q.; Li, L.; Wu, P.; Xu, N.; Wang, L.; Li, M.; Dai, A.; Amine, K.; Mai, L.; Lu, J. Silica Restricting the Sulfur Volatilization of Nickel Sulfide for High-Performance Lithium-Ion Batteries. *Adv. Energy Mater.* **2019**, *9*, No. 1901153.

(3) Jin, Y.; Zhu, B.; Lu, Z.; Liu, N.; Zhu, J. Challenges and Recent Progress in the Development of Si Anodes for Lithium-Ion Battery. *Adv. Energy Mater.* **2017**, *7*, No. 1700715.

(4) Dunn, B.; Kamath, H.; Tarascon, J.-M. Electrical Energy Storage for the Grid: A Battery of Choices. *Science* **2011**, *334*, 928−935.

(5) Jia, H.; Zheng, J.; Song, J.; Luo, L.; Yi, R.; Estevez, L.; Zhao, W.; Patel, R.; Li, X.; Zhang, J.-G. A novel approach to synthesize micrometer-sized porous silicon as a high performance anode for lithium-ion batteries. *Nano Energy* **2018**, *50*, 589−597.

(6) Liu, S.; Li, F.; Wang, D.; Huang, C.; Zhao, Y.; Baek, J.-B.; Xu, J. 3D Macroporous Mo_xC@N-C with Incorporated Mo Vacancies as Anodes for High-Performance Lithium-Ion Batteries. *Small Methods* **2018**, *2*, No. 1800040.

(7) Wang, J.; Zhou, M.; Tan, G.; Chen, S.; Wu, F.; Lu, J.; Amine, K. Encapsulating Micro-Nano Si/SiOx into Conjugated Nitrogen-Doped Carbon as Binder-Free Monolithic Anodes for Advanced Lithium Ion Batteries. *Nanoscale* **2015**, *7*, 8023−8034.

(8) Bao, W.; Wang, J.; Chen, S.; Li, W.; Su, Y.; Wu, F.; Tan, G.; Lu, J. Three-Dimensional Hierarchical Structure of Cyclized-PAN/Si/Ni for Mechanically Stable Silicon Anodes. *J. Mater. Chem. A* **2017**, *5*, 24667−24676.

(9) Mishra, K.; Zheng, J.; Patel, R.; Estevez, L.; Jia, H.; Luo, L.; El-Khoury, P. Z.; Li, X.; Zhou, X.-D.; Zhang, J.-G. High performance porous Si@C anodes synthesized by low temperature aluminothermic reaction. *Electrochim. Acta* **2018**, *269*, 509−516.

(10) Jiang, S.; Hu, B.; Sahore, R.; Zhang, L.; Liu, H.; Zhang, L.; Lu, W.; Zhao, B.; Zhang, Z. Surface-Functionalized Silicon Nanoparticles as Anode Material for Lithium-Ion Battery. *ACS Appl. Mater. Interfaces* **2018**, *10*, 44924−44931.

(11) Chen, H.; Xu, H.; Zeng, Y.; Ma, T.; Wang, W.; Liu, L.; Wang, F.; Zhang, X.; Qiu, X. Quantification on Growing Mass of Solid Electrolyte Interphase and Deposited Mn(II) on the Silicon Anode of $LiMn_2O_4$ Full Lithium-Ion Cells. *ACS Appl. Mater. Interfaces* **2019**, *11*, 27839−27845.

(12) Tang, D.; Yu, H.; Zhao, J.; Liu, W.; Zhang, W.; Miao, S.; Qiao, Z.-A.; Song, J.; Zhao, Z. Bottom-up synthesis of mesoporous germanium as anodes for lithium-ion batteries. *J. Colloid Interface Sci. 561*, 494 500. DOI: 10.1016/j.jcis.2019.11.024.

(13) Im, H. S.; Cho, Y. J.; Lim, Y. R.; Jung, C. S.; Jang, D. M.; Park, J.; Shojaei, F.; Kang, H. S. Phase Evolution of Tin Nanocrystals in Lithium Ion Batteries. *ACS Nano* **2013**, *7*, 11103−11111.

(14) Sun, Y.; Liu, N.; Cui, Y. Promises and challenges of nanomaterials for lithium-based rechargeable batteries. *Nat. Energy* **2016**, *1*, No. 16071.

(15) Yin, Y.; Wan, L.; Guo, Y. Silicon-based nanomaterials for lithium-ion batteries. *Chin. Sci. Bull.* **2012**, *57*, 4104−4110.

(16) Liu, X. H.; Zhong, L.; Huang, S.; Mao, S. X.; Zhu, T.; Huang, J. Y. Size-Dependent Fracture of Silicon Nanoparticles During Lithiation. *ACS Nano* **2012**, *6*, 1522−1531.

(17) Gao, S.; Yang, D.; Pan, Y.; Geng, Li.; Li, S.; Li, X.; Cao, P.-F.; Yang, H. From natural material to high-performance silicon based anode: Towards cost-efficient silicon based electrodes in high-performance Li-ion batteries. *Electrochim. Acta* **2019**, *327*, No. 135058.

(18) Liu, S.; Zhang, X.; Yan, P.; Cheng, R.; Tang, Y.; Cui, M.; Wang, B.; Zhang, L.; Wang, X.; Jiang, Y.; Wang, L.; Yu, H. Dual Bond Enhanced Multidimensional Constructed Composite Silicon Anode for High-Performance Lithium Ion Batteries. *ACS Nano* **2019**, *13*, 8854−8864.

(19) Geng, Li.; Yang, D.; Gao, S.; Zhang, Z.; Sun, F.; Pan, Y.; Li, S.; Li, X.; Cao, P.-F.; Yang, H. Facile Fabrication of Porous Si Microspheres from Low-Cost Precursors for High-Capacity Electrode. *Adv. Mater. Interfaces* **2019**, *7*, No. 1901726.

(20) Zhang, C.; Gu, L.; Kaskhedikar, N.; Gui, G.; Maier, J. Preparation of Silicon@Silicon Oxide Core−Shell Nanowires from a Silica Precursor toward a High Energy Density Li-Ion Battery Anode. *ACS Appl. Mater. Interfaces* **2013**, *5*, 12340−12345.

(21) Park, M.-H.; Kim, M. G.; Joo, J.; Kim, K.; Kim, J.; Ahn, S.; Cui, Y.; Cho, J. Silicon Nanotube Battery Anodes. *Nano Lett.* **2009**, *9*, 3844−3847.

(22) Abel, P. R.; Chockla, A. M.; Lin, Y.-M.; Holmberg, V. C.; Harris, J. T.; Korgel, B. A.; Heller, A.; Mullins, C. B. Nanostructured Si(1-x)Gex for Tunable Thin Film Lithium-Ion Battery Anodes. *ACS Nano* **2013**, *7*, 2249−2257.

(23) Jiménez, A. R.; Klöpsch, R.; Wagner, R.; Rodehorst, U. C.; Kolek, M.; Nölle, R.; Winter, M.; Placke, T. A Step toward High-

Energy Silicon-Based Thin Film Lithium Ion Batteries. *ACS Nano* **2017**, *11*, 4731−4744.
(24) Qiang, Z.; Liu, X.; Zou, F.; Cavicchi, K.; Zhu, Y.; Vogt, B. Bimodal Porous Carbon-Silica Nanocomposites for Li-Ion Batteries. *J. Phys. Chem. C* **2017**, *121*, 16702−16709.
(25) Munaoka, T.; Yan, X.; Lopez, J.; To, J. W. F.; Park, J.; Tok, J. B.-H.; Cui, Y.; Bao, Z. Ionically Conductive Self-Healing Binder for Low Cost Si Microparticles Anodes in Li-Ion Batteries. *Adv. Energy Mater.* **2018**, *8*, No. 1703138.
(26) Pan, Y.; Gao, S.; Sun, F.; Yang, H.; Cao, P.-F. Polymer Binders Constructed through Dynamic Noncovalent Bondsfor High-Capacity Silicon-Based Anodes. *Chem. - Eur. J.* **2019**, *25*, 10976−10994.
(27) Liu, G.; Xun, S.; Vukmirovic, N.; Song, X.; Olalde-Velasco, P.; Zheng, H.; Battaglia, V. S.; Wang, L.; Yang, W. Polymers with Tailored Electronic Structure for High Capacity Lithium Battery Electrodes. *Adv. Mater.* **2011**, *23*, 4679−4683.
(28) Magasinski, A.; Zdyrko, B.; Kovalenko, I.; Hertzberg, B.; Burtovyy, R.; Huebner, C. F.; Fuller, T. F.; Luzinov, I.; Yushin, G. Toward Efficient Binders for Li-Ion Battery Si-Based Anodes: Polyacrylic Acid. *ACS Appl. Mater. Interfaces* **2010**, *2*, 3004−3010.
(29) Hu, B.; Jiang, S.; Shkrob, I. A.; Zhang, J.; Trask, S. E.; Polzin, B. J.; Jansen, A.; Chen, W.; Liao, C.; Zhang, Z.; Zhang, L. Understanding of pre-lithiation of poly(acrylic acid) binder: Striking the balances between the cycling performance and slurry stability for silicon-graphite composite electrodes in Li-ion batteries. *J. Power Sources* **2019**, *416*, 125−131.
(30) Lestriez, B.; Bahri, S.; Sandu, I.; Roue, L.; Guyomard, D. On the binding mechanism of CMC in Si negative electrodes for Li-ion batteries. *Electrochem. Commun.* **2007**, *9*, 2801−2806.
(31) Park, Y.; Lee, S.; Kim, S.-H.; Jang, B. Y.; Kim, J. S.; Oh, S. M.; Kim, J.-Y.; Choi, N.-S.; Lee, K. T.; Kim, B.-S. A photo-cross-linkable polymeric binder for silicon anodes in lithium ion batteries. *RSC Adv.* **2013**, *3*, 12625−12630.
(32) Kim, J. S.; Choi, W.; Cho, K. Y.; Byun, D.; Lim, J.; Lee, J. K. Effect of polyimide binder on electrochemical characteristics of surface-modified silicon anode for lithium ion batteries. *J. Power Sources* **2013**, *244*, 521−526.
(33) Luo, L.; Xu, Y.; Zhang, H.; Han, X.; Dong, H.; Xu, X.; Chen, C.; Zhang, Y.; Lin, J. Comprehensive Understanding of High Polar Polyacrylonitrile as an Effective Binder for Li-Ion Battery Nano-Si Anodes. *ACS Appl. Mater. Interfaces* **2016**, *8*, 8154−8161.
(34) Komaba, S.; Shimomura, K.; Yabuuchi, N.; Ozeki, T.; Yui, H.; Konno, K. Study on Polymer Binders for High-Capacity SiO Negative Electrode of Li-Ion Batteries. *J. Phys. Chem. C* **2011**, *115*, 13487−13495.
(35) Chen, C.; Lee, S. H.; Cho, M.; Kim, J.; Lee, Y. Cross-Linked Chitosan as an Efficient Binder for Si Anode of Li-ion Batteries. *ACS Appl. Mater. Interfaces* **2016**, *8*, 2658−2665.
(36) Liu, J.; Zhang, Q.; Zhang, T.; Li, J.-T.; Huang, L.; Sun, S.-G. A Robust Ion-Conductive Biopolymer as a Binder for Si Anodes of Lithium-Ion Batteries. *Adv. Funct. Mater.* **2015**, *25*, 3599−3605.
(37) Kang, S.; Yang, K.; White, S. R.; Sottos, N. R. Silicon Composite Electrodes with Dynamic Ionic Bonding. *Adv. Energy Mater.* **2017**, *7*, No. 1700045.
(38) Song, J.; Zhou, M.; Yi, R.; Xu, T.; Gordin, M. L.; Tang, D.; Yu, Z.; Regula, M.; Wang, D. Interpenetrated Gel Polymer Binder for High-Performance Silicon Anodes in Lithium-ion Batteries. *Adv. Funct. Mater.* **2014**, *24*, 5904−5910.
(39) Cao, P.-F.; Yang, G.; Li, B.; Zhang, Y.; Zhao, S.; Zhang, S.; Erwin, A.; Zhang, Z.; Sokolov, A. P.; Nanda, J.; Saito, T. Rational Design of a Multifunctional Binder for High-Capacity Silicon-Based Anodes. *ACS Energy Lett.* **2019**, *4*, 1171−1180.
(40) Mizutani, K.; Hongo, C.; Matsumoto, T.; Nishino, T. Acrylic pressure-sensitive adhesives with nanodiamonds and acid−base dependence of the pressure-sensitive adhesive properties. *J. Appl. Polym. Sci.* **2018**, *135*, No. 46349.
(41) Sun, S.; Li, M.; Liu, A. A review on mechanical properties of pressure sensitive adhesives. *Int. J. Adhes. Adhes.* **2013**, *41*, 98−106.
(42) Schindler, M.; Koller, M.; Muller-Buschbaum, P. Pressure-Sensitive Adhesives under the Influence of Relative Humidity: Inner Structure and Failure Mechanisms. *ACS Appl. Mater. Interfaces* **2015**, *7*, 12319−12327.
(43) Creton, C.; Ciccotti, M. Fracture and adhesion of soft materials: a review. *Rep. Prog. Phys.* **2016**, *79*, No. 046601.
(44) Kim, S.; Jeong, Y. K.; Wang, Y.; Lee, H.; Choi, J. W. A "Sticky" Mucin-Inspired DNA-Polysaccharide Binder for Silicon and Silicon−Graphite Blended Anodes in Lithium-Ion Batteries. *Adv. Mater.* **2018**, *30*, No. 1707594.
(45) Karnal, P.; Roberts, P.; Gryska, S.; King, C.; Barrios, C.; Frechette, J. Importance of Substrate Functionality on the Adhesion and Debonding of a Pressure-Sensitive Adhesive under Water. *ACS Appl. Mater. Interfaces* **2017**, *9*, 42344−42353.
(46) Cao, P.-F.; Naguib, M.; Du, Z.; Stacy, E.; Li, B.; Hong, T.; Xing, K.; Voylov, D. N.; Li, J.; Wood, D. L., III; Sokolov, A. P.; Nanda, J.; Saito, T. Effect of Binder Architecture on the Performance of Silicon/Graphite Composite Anodes for Lithium Ion Batteries. *ACS Appl. Mater. Interfaces* **2018**, *10*, 3470−3478.
(47) Giannozzi, P.; Baroni, S.; Bonini, N.; Calandra, M.; Car, R.; Cavazzoni, C.; Ceresoli, D.; Chiarotti, G. L.; Cococcioni, M.; Dabo, N.; Corso, A. D.; Gironcoli, S.; Fabris, S.; Fratesi, G.; Gebauer, R.; Gerstmann, U.; Gougoussis, C.; Kokalj, A.; Lazzeri, M.; Martin-Samos, L.; Marzari, N.; Mauri, F.; Mazzarello, R.; Paolini, S.; Pasquarello, A.; Paulatto, L.; Sbraccia, C.; Scandolo, S.; Sclauzero, G.; Seitsonen, A. P.; Smogunov, A.; Umari, P.; Wentzcovitch, R. M. QUANTUM ESPRESSO: a modular and open-source software project for quantum simulations of materials. *J. Phys.: Condens. Matter* **2009**, *21*, No. 395502.
(48) Becke, A. D. Density-fnnctional exchange-energy approximation with correct asymptotic behavior. *Phys. Rev. A* **1988**, *38*, 3098−3100.
(49) Lee, C.; Yang, W.; Parr, R. G. Development of the Colic-Salvetti correlation-energy formula into a functional of the electron density. *Phys. Rev. B: Condens. Matter* **1988**, *37*, 785−789.
(50) Roy, S.; Freiberg, S.; Leblanc, C.; Hore, D. K. Surface Structure of Acrylate Polymer Adhesives. *Langmuir* **2017**, *33*, 1763−1768.
(51) Yuca, N.; Zhao, H.; Song, X.; Dogdu, M. F.; Yuan, W.; Fu, Y.; Battaglia, V. S.; Xiao, X.; Liu, G. A Systematic Investigation of Polymer Binder Flexibility on the Electrode Performance of Lithium-Ion Batteries. *ACS Appl. Mater. Interfaces* **2014**, *6*, 17111−17118.
(52) Cordier, P.; Tournilhac, F.; Soulie-Ziakovic, C.; Leibler, L. Self-mending and thermoreversible rubber from supramolecular assembly. *Nature* **2008**, *451*, 977−980.
(53) Lopez, J.; Chen, Z.; Wang, C.; Andrews, C.; Cui, Y.; Bao, Z. The Effects of Cross-Linking in a Supramolecular Binder on Cycle Life in Silicon Microparticle Anodes. *ACS Appl. Mater. Interfaces* **2016**, *8*, 2318−2324.
(54) Zhu, X.; Zhang, F.; Zhang, L.; Zhang, L.; Song, Y.; Jiang, T.; Sayed, S.; Lu, C.; Wang, X.; Sun, J.; Liu, Z. A Highly Stretchable Cross-Linked Polyacrylamide Hydrogel as an Effective Binder for Silicon and Sulfur Electrodes toward Durable Lithium-Ion Storage. *Adv. Funct. Mater.* **2018**, *28*, No. 1705015.
(55) Kovalenko, I.; Zdyrko, B.; Magasinski, A.; Hertzberg, B.; Milicev, Z.; Burtovyy, R.; Luzinov, I.; Yushin, G. A Major Constituent of Brown Algae for Use in High-Capacity Li-Ion Batteries. *Science* **2011**, *334*, 75−79.
(56) Higgins, T. M.; Park, S. H.; King, P. J.; Zhang, C. J.; McEvoy, N.; Berner, N. C.; Daly, D.; Shmeliov, A.; Khan, U.; Duesberg, G.; Nicolosi, V.; Coleman, J. N. A Commercial Conducting Polymer as Both Binder and Conductive Additive for Silicon Nanoparticle-Based Lithium-Ion Battery Negative Electrodes. *ACS Nano* **2016**, *10*, 3702−3713.
(57) Feng, K.; Li, M.; Liu, W.; Kashkooli, A. G.; Xiao, X.; Cai, M.; Chen, Z. Silicon-Based Anodes for Lithium-Ion Batteries: From Fundamentals to Practical Applications. *Small* **2018**, *14*, No. 1702737.
(58) Hwang, G.; Kim, J.-M.; Hong, D.; Kim, C.-K.; Choi, N.-S.; Lee, S.-Y.; Park, S. Multifunctional natural agarose as an alternative

https://dx.doi.org/10.1021/acsaem.9b02420
ACS Appl. Energy Mater. 2020, 3, 3387−3396

material for high-performance rechargeable lithium-ion batteries. *Green Chem.* **2016**, *18*, 2710−2716.
(59) Taghizadeh, S. M.; Ghasemi, D. Rheological and Adhesion Properties of Acrylic Pressure-Sensitive Adhesives. *J. Appl. Polym. Sci.* **2011**, *120*, 411−418.
(60) Nguyen, C. C.; Yoon, T.; Seo, D. M.; Guduru, P.; Lucht, B. L. Systematic Investigation of Binders for Silicon Anodes: Interactions of Binder with Silicon Particles and Electrolytes and Effects of Binders on Solid Electrolyte Interphase Formation. *ACS Appl. Mater. Interfaces* **2016**, *8*, 12211−12220.
(61) Lim, S.; Chu, H.; Lee, K.; Yim, T.; Kim, Y.-J.; Mun, J.; Kim, T.-H. Physically Cross-linked Polymer Binder Induced by Reversible Acid-Base Interaction for High-Performance Silicon Composite Anodes. *ACS Appl. Mater. Interfaces* **2015**, *7*, 23545−23553.

https://dx.doi.org/10.1021/acsaem.9b02420
ACS Appl. Energy Mater. 2020, 3, 3387−3396